



Surface oxidation of PAN-based ultrahigh modulus carbon fibers (UHMCFs) and its effect on the properties of UHMCF/EP composites

Xinyu Wang¹ · Xin Qian² · Yonggang Zhang² · Xuefei Wang² · Shulin Song² · Cheng Zhang¹

Received: 31 March 2020 / Revised: 5 July 2020 / Accepted: 30 July 2020 / Published online: 9 August 2020
© Korean Carbon Society 2020

Abstract

In this study, nitric acid oxidation with varied treatment temperature and time was conducted on the surfaces of polyacrylonitrile-based ultrahigh modulus carbon fibers. Scanning electron microscopy, X-ray photoelectron spectroscopy, Raman spectroscopy and surface tension/dynamic contact angle instruments were used to investigate changes in surface topography and chemical functionality before and after surface treatment. Results showed that the nitric acid oxidation of ultrahigh modulus carbon fibers resulted in decreases in the values of the crystallite thickness L_c and graphitization degree. Meanwhile, increased treating temperature and time made the decreases more obviously. The surfaces of ultrahigh modulus carbon fibers became much more activity and functionality after surface oxidation, e.g., the total surface energy of oxidized samples at 80 °C for 1 h increased by 27.7% compared with untreated fibers. Effects of surface nitric acid oxidation on the mechanical properties of ultrahigh modulus carbon fibers and its reinforced epoxy composites were also researched. Significant decreases happened to the tensile modulus of fibers due to decreased L_c value after the nitric acid oxidation. However, surface treatment had little effect on the tensile strength even as the treating temperature and processing time increased. The highest interfacial shear strength of ultrahigh modulus carbon fibers/epoxy composites increased by 25.7% after the nitric acid oxidation. In the final, surface oxidative mechanism of ultrahigh modulus carbon fibers in the nitric acid oxidation was studied. Different trends of the tensile strength and tensile modulus of fibers in the nitric acid oxidation resulted from the typical skin–core structure.

Keywords Ultrahigh modulus carbon fiber · Nitric acid treatment · Microstructure · Surface activity

1 Introduction

During the past decades, carbon fiber reinforced polymers (CFRPs) have been widely used owing to their excellent ratio of stiffness to material density and the advantages of designing composite structures for optimum in-service performance [1–6]. The properties of CFRPs are greatly governed by the properties of carbon fibers and resin matrix as well as the interface between them. The strong interface

between carbon fibers and the matrix can effectively transfer foreign load from the matrix to the fibers, which enhances the structural integrity of CFRPs and improves their performance [7–9].

However, carbon fibers usually have highly inert surfaces due to high-temperature treatment in its preparation process. To improve surface chemical reactivity, the surface treatment of carbon fibers become necessary and it can be classified into two categories: surface coating method and surface oxidation method [10, 11]. The surface coating method is to improve the bonding ability of carbon fibers by directly coating or growing active material on fiber surfaces, such as electrochemical polymerization [12, 13], in-situ growth of carbon material [14, 15] and the introduction of nanoparticles [16–19].

Surface oxidation also can be divided into electrochemical oxidation [3, 20, 21], liquid-phase oxidation [9, 22], gas-phase (plasma) oxidation [23–26], etc. In the process of liquid-phase oxidation, nitric acid, sulfuric acid, phosphoric acid, and hydrogen peroxide can be chosen as the oxidizing

✉ Xin Qian
qx3023@nimte.ac.cn

✉ Cheng Zhang
czhang@sit.edu.cn

¹ School of Materials Science and Engineering, Shanghai Institute of Technology, Shanghai 201418, China

² National Engineering Laboratory of Carbon Fiber Preparation Technology, Ningbo Institute of Materials Technology and Engineering, Chinese Academy of Sciences, Ningbo 315201, Zhejiang, China

agent. Yue et al. [9] indicated that surface treatment of carbon fibers by HNO₃ could improve the mechanical properties of carbon fiber reinforced composites. According to the study by Woodhead et al. [27], much more functional groups of C=O and NO_x were introduced onto the surface of carbon fibers after HNO₃ oxidation treatment.

According to the tensile modulus, PAN-based carbon fibers can be roughly classified into four grades: standard grade carbon fibers (230–240 GPa), high strength and intermediate modulus carbon fibers (HSCFs, 280–300 GPa), high strength and high modulus carbon fibers (HMCfFs, 350–480 GPa) and ultra-high modulus carbon fibers (UHMCFs, more than 480 GPa) [28–30].

Compared with HSCFs, the surfaces of HMCfFs and UHMCFs are much more inert due to the high-temperature graphitization process with a heat-treatment temperature of 2000 °C. Especially for the UHMCFs, the heat-treatment temperature is almost 3000 °C. Increased fiber tensile modulus and surface inertness of HMCfFs and UHMCFs also result in weak interfacial strength between carbon fiber and resin matrix. A few researches have been studied on the surface treatments of low-modulus carbon fibers and HMCfFs [31–35]. However, the study on surface oxidation of UHMCFs is very limited. In our recent published article, the surfaces of UHMCFs were electrochemically oxidized and the corresponding stepwise oxidation mechanism of UHMCFs in the electrochemical modification was revealed [30].

HNO₃ oxidation can effectively create functional groups on carbon fiber surfaces. Therefore, the specific effect of HNO₃ oxidation on the microstructure and mechanical properties of UHMCFs was explored in the present research. Scanning electron microscopy (SEM), X-ray diffraction (XRD), X-ray photoelectron spectroscopy (XPS), Raman spectroscopy (Raman) and dynamic contact angle analyzer/surface tension device were utilized to reveal changes in surface physico-chemical structure of UHMCFs during the HNO₃ oxidation. The mechanical properties of single filament and the interfacial shear strength (IFSS) between carbon fibers and epoxy resin were also researched.

2 Experimental

2.1 Materials

The ultra-high modulus carbon fibers (UHMCFs) in this study were PAN-based carbon fibers and produced in our laboratory, with the tensile strength of 3.39 GPa and tensile modulus of 493.65 GPa. The typical diameter of single filament was about 5 μm. The UHMCFs without surface treatment and sizing process were collected immediately after high-temperature graphitization. HNO₃ of analytical pure was supplied by Sinopharm Chemical Reagent Co. Ltd.

2.2 HNO₃ oxidation of UHMCFs

Surface treatment of UHMCFs was carried out by dipping carbon fiber into the HNO₃ solution. Firstly, the fiber samples with the length of about 50 mm were immersed in HNO₃ solution. Secondly, the surface treated samples were filtered with deionized water followed by a further ultrasonic washing for 0.5 h. Thirdly, the samples were dried in the oven for 6 h with the temperature of 50 °C.

The time for the samples immersed in HNO₃ solution were 0.5 h, 1 h and 2 h, respectively. The processing temperature of HNO₃ solution were room temperature 25 °C, 60 °C and 80 °C, respectively. According to the treating time and temperature, the corresponding samples were named as CF-HNO₃-25 °C-0.5 h/1 h/2 h, CF-HNO₃-60 °C-0.5 h/1 h/2 h, and CF-HNO₃-80 °C-0.5 h/1 h/2 h, respectively. UHMCFs without any treatment (CF-untreated) were also prepared as the comparative sample.

2.3 Characterization

2.3.1 Surface morphology characterization

The surface morphologies of UHMCFs before and after HNO₃ oxidation were characterized by Hitachi S-4800 model scanning electron microscope (SEM), with an amplification of 15,000 times. The fiber samples were secured on a metal mount by conducting tape and then coated with gold prior to examination.

2.3.2 Crystal structure analysis

A D8 ADVANCE DAVINCI X-ray diffractometer (XRD) was used to characterize the crystal structure of UHMCFs with Cu Kα radiation (= 1.5406 nm) generated at 40 kV and 40 mA. XRD patterns were collected at 2°/min in a 2θ range of 10°–35°. The crystallite thickness was calculated according to Scherrer equation [36]:

$$L_c = \frac{k\lambda}{\beta \cos \theta}, \quad (1)$$

where L_c is the crystallite thickness, K is Scherrer constant, 0.9, λ is the wavelength of the incident X-ray, 0.15418 nm, 2θ is the diffraction angle and β is the half-height-width of the diffraction peak.

2.3.3 Surface chemical microstructure

The surface chemical microstructure of UHMCFs was characterized by a Renishaw inVia Reflex Raman spectrometer with a green 532 nm line of an argon ion laser as the

incident radiation. The Raman spectra were collected with the wavenumber range of 1000–2000 cm^{-1} under nitrogen atmosphere.

2.3.4 Surface chemical compositions

The surface chemical elements of UHMCFs were analyzed by an Axis Ultradld model X-ray photoelectron spectroscopy (XPS) with an achromatic Mg K α X-ray as a radiation source. The discharge stream was with a current of 30 mA and a voltage of 15 kV. The total pressure in the main vacuum chamber was below 10^{-8} mbar. Data processing was performed using Casa XPS processing software and all binding energies were referred to the C $_{1s}$ peak at 284.6 eV.

2.3.5 Surface wettability

Dynamic contact angle measurements were performed using a DCAT21 model dynamic contact angle meter (Data Physics Instruments, Germany). Deionized water ($\gamma_1=72.8$ mN/m, $\gamma^d=21.8$ mN/m, $\gamma^p=51.0$ mN/m) and diiodomethane ($\gamma_1=50.8$ mN/m, $\gamma^d=50.8$ mN/m) [10, 37, 38] were selected as the tested liquids. The contact angle can be determined by the Wilhelmy formula:

$$\cos \theta = \frac{mg}{\Pi \cdot d_f \cdot \gamma_1}, \quad (2)$$

where d_f is the fiber diameter, g is the gravitational acceleration, and γ_1 is the surface energy of the test liquid. The surface energy of UHMCFs (γ_f) can be calculated through the following equations [11, 13]:

$$\gamma_f(1 + \cos \theta) = 2(\gamma_1^p \gamma_f^p)^{1/2} + 2(\gamma_1^d \gamma_f^d)^{1/2}, \quad (3)$$

$$\gamma_f = \gamma_f^p + \gamma_f^d, \quad (4)$$

where γ_1^p, γ_1^d are the polarity component and dispersion component of the test fluid, respectively; γ_f^p, γ_f^d are the polarity component and dispersion component of carbon fiber, respectively.

2.3.6 Mechanical properties of UHMCFs and interfacial property of carbon fiber reinforced epoxy composite

The tensile tests of carbon fibers were performed on a FAVI-MAT+ single fiber analyzer (Textechno H. Stein, Germany) according to the ASTM D3379-75 standard. The tensile load-elongation curves were collected at a test speed of 2.0 mm/min with the gauge length of 25 mm. The results were analyzed using Weibull statistical methods and more than 30 filaments for each specimen were tested.

The interfacial shear strength (IFSS) of carbon fiber reinforced epoxy composite were characterized by the microbond test [26]. Single filament in fiber tows was picked out with the length of 30 mm and secured onto the metal plate with superglue. A mixture of E-44 epoxy resin and triethylenetetramine with a weight ratio of 10:1 was dropped onto the single fiber tow to form several resin droplets. The droplets were then cured at the 120 °C for 2 h. The IFSS between UHMCFs and epoxy resin matrix was detected by an interfacial microbond assessment instrument (Model HM410, Tohei Sanyon Co., Japan) and calculated according to the following equation:

$$\text{IFSS} = \frac{F_{\max}}{\pi dl}, \quad (5)$$

where F_{\max} is the maximal load as the interfacial debonding or sliding occurs, d is the fiber diameter, and l is the embedded length of the epoxy droplet.

3 Results and discussion

3.1 Surface morphology analysis by SEM

The morphology of carbon fibers treated with HNO $_3$ (processing time 1 h) are shown in Fig. 1. Well-defined longitudinal ridges and striations running along the fibers' axis were found on the surfaces of untreated UHMCFs (Fig. 1a), which resulted from the wet spinning process in the preparation of PAN-precursors [39]. Compared with untreated UHMCFs, changes in the longitudinal ridges and striations on the surfaces of CF-HNO $_3$ -25 °C were not obvious (Fig. 1b). However, UHMCF surfaces became smoother rather than rougher as the treating temperature increased to 60 °C and 80 °C (Fig. 1c, d). The reason possibly lied in that the ridges of longitudinal grooves were oxidized much more intensively than the bottoms due to their large areas [21]. The violent oxidation at higher temperature finally damaged the groove structure which made the grooves less rougher.

3.2 XRD analysis

XRD patterns of UHMCFs before and after HNO $_3$ oxidation (processing time 1 h) are shown in Fig. 2. As can be seen, the diffraction peak located at 26° in all the curves are assigned to the 002 peak [40–42]. The existence of the 002 peak is attributed to the typical turbostratic structure of carbon and it reveals that there also exists imperfect graphite structure in the UHMCFs. By comparison of XRD patterns of untreated UHMCFs, the full-width at half-maxima (FWHM) of the 002 peak increased in the XRD patterns of

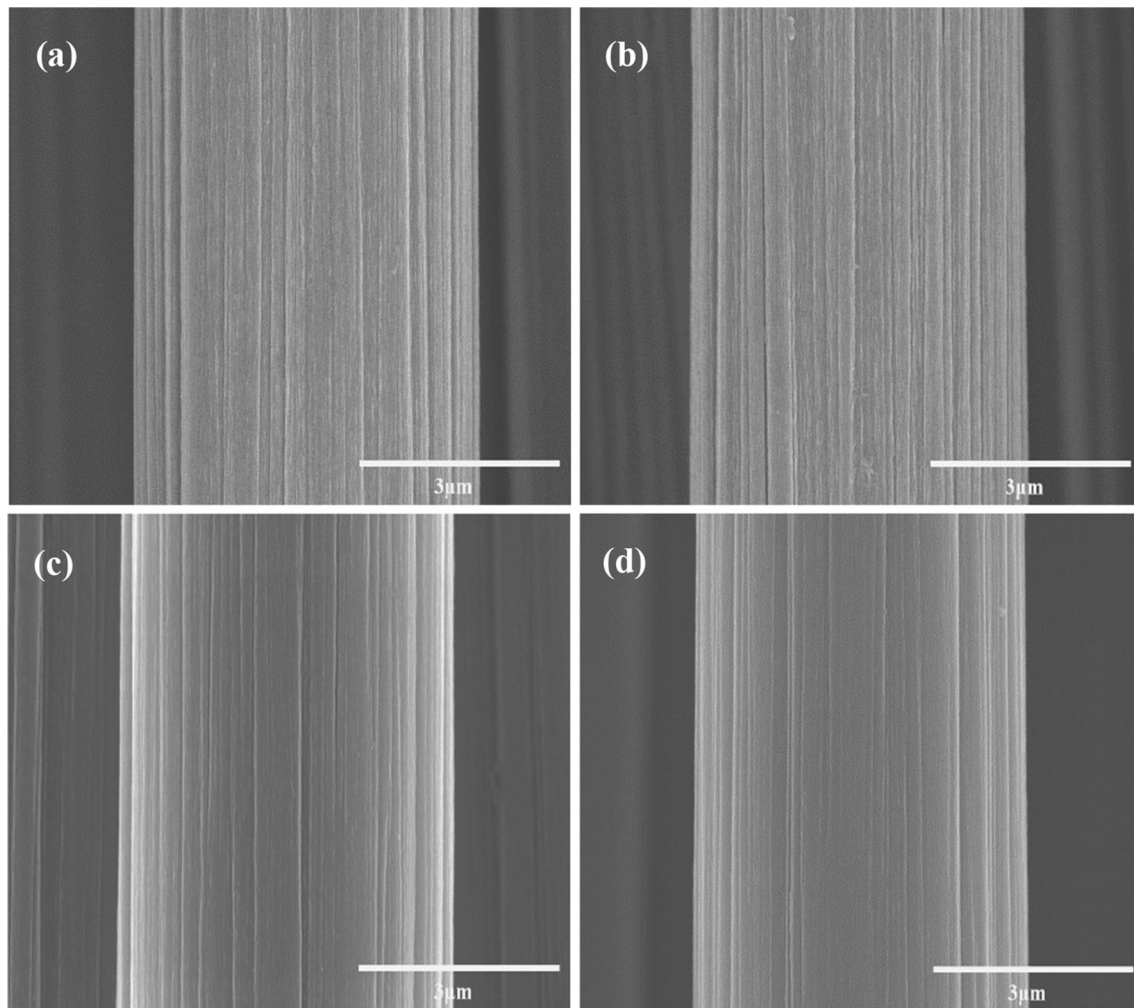


Fig. 1 SEM micrographs of UHMCFs: **a** CF-untreated, **b** CF-HNO₃-25 °C-1 h, **c** CF-HNO₃-60 °C-1 h, **d** CF-HNO₃-80 °C-1 h

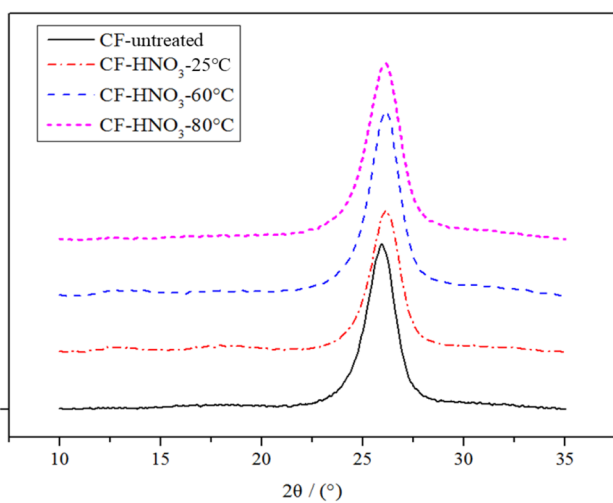


Fig. 2 XRD patterns of UHMCFs before and after the HNO₃ oxidation

Table 1 XRD spectrum parameters of UHMCFs under HNO₃ treatment

Samples	2θ (°)	d_{002} (nm)	FWHM (°)	Lc (nm)
CF-untreated	25.95	0.3430	0.965	8.46
CF-HNO ₃ -25 °C-0.5 h	26.09	0.3413	0.969	8.42
CF-HNO ₃ -60 °C-0.5 h	26.02	0.3422	0.976	8.36
CF-HNO ₃ -80 °C-0.5 h	26.12	0.3409	0.982	8.31
CF-HNO ₃ -25 °C-1 h	26.14	0.3406	0.970	8.41
CF-HNO ₃ -60 °C-1 h	26.11	0.3410	0.985	8.29
CF-HNO ₃ -80 °C-1 h	26.08	0.3413	0.994	8.21
CF-HNO ₃ -25 °C-2 h	26.09	0.3413	0.972	8.40
CF-HNO ₃ -60 °C-2 h	26.12	0.3412	0.992	8.23
CF-HNO ₃ -80 °C-2 h	26.15	0.3406	1.005	8.12

surface oxidized UHMCFs, which indicated HNO_3 oxidation had destroyed the original crystal structure of the fibers.

The calculated XRD spectrum parameters of UHMCFs before and after HNO_3 oxidation are provided in Table 1. The average interlayer spacing (d_{002}) of untreated UHMCFs was 0.3430 nm which was slightly higher than the d_{002} value of the ideal graphite crystal (0.3354 nm). Compared with untreated UHMCFs, all the d_{002} value after surface treatment with HNO_3 decreased, and the HNO_3 oxidation of UHMCFs also resulted in increased values of FWHM and decreased values of the crystallite thickness L_c . This result showed that the HNO_3 oxidation temperature of UHMCFs could affect graphite microcrystalline structure.

Figure 3 shows the relationship between the crystallite thickness L_c and the processing time and temperature. When the processing temperature remained the same, the L_c value of oxidized UHMCFs decreased with the increase of the processing time. However, decreases in the L_c values of oxidized UHMCFs were not obvious as the processing temperature was at room temperature 25 °C, e.g., the L_c value of CF- HNO_3 -25 °C-2 h was still 8.40 nm (as shown in Table 1).

Results in the paper also showed that increased processing time and temperature could result in significant decreases in the L_c value. When the process temperature of HNO_3 oxidation was 80 °C, the L_c values of CF- HNO_3 -80 °C-0.5 h, CF- HNO_3 -80 °C-1 h, and CF- HNO_3 -80 °C-2 h samples (as shown in Table 1) decreased by 1.7%, 3.0% and 4.0% compared with that of untreated UHMCFs, respectively.

3.3 Raman spectroscopy analysis

Raman spectroscopy has been proved to be an effective method to follow the micromechanics of deformation of CF surfaces [43, 44]. Figure 4 reveals the Raman spectra

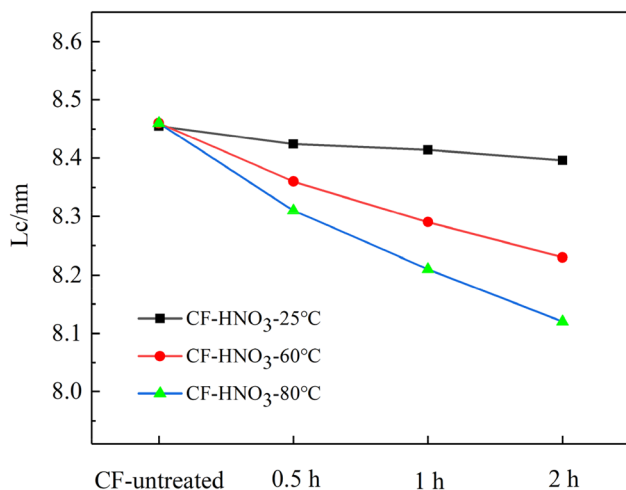


Fig. 3 Relationship between crystallite thickness L_c , the processing time and the temperature of HNO_3 oxidation

and their corresponding fitting curves of UHMCFs before and after the HNO_3 oxidation (processing time 1 h) over the 1000–2100 cm^{-1} frequency range. Two characteristic bands can be found in the Raman spectra of all samples. The D-band located at around 1350 cm^{-1} is assigned to increased crystallite boundaries and the G-band (about 1580 cm^{-1}) is assigned to the E_{2g} vibrational mode of the graphite crystal. The intensity ratio of two bands I_D/I_G has been utilized to characterize the degree of structural disorder [45]. Besides the G-band and D-band, another peak D'-band around 1620 cm^{-1} is also observed in the Raman spectra of UHMCFs. The D'-band resulted from disorder and small crystallite structure are also defect-induced Raman features [46].

Table 2 reveals the peak position and FWHM values of the disorder D-line and graphitic G-line, as well as the I_D/I_G ratios. As can be seen, the I_D/I_G ratios of HNO_3 oxidized UHMCFs were higher than that of untreated sample, and the higher the processing temperature in the HNO_3 oxidation, the higher the I_D/I_G ratio. Increased I_D/I_G ratios after the HNO_3 oxidation indicated that surface structure of oxidized UHMCFs became much more disorder. As a result, the chemical etching and increased number active carbon atoms of during the HNO_3 oxidation could reduce the graphitization degree of UHMCFs, which was consistent with the results by XRD.

According to above results in Table 2, higher processing temperature could result in increased I_D/I_G values on the surfaces of oxidized UHMCFs. The relationship between the I_D/I_G values, the processing time and treatment temperature is shown in Fig. 5. As can be seen, a higher processing time also led to significant increases in the I_D/I_G values. Compared with the I_D/I_G value of untreated UHMCFs (0.528), the I_D/I_G values of CF- HNO_3 -80 °C-0.5 h, CF- HNO_3 -80 °C-1 h, and CF- HNO_3 -80 °C-2 h samples (as shown in Table 2) increased to 0.550, 0.565 and 0.585, respectively. The I_D/I_G values of CF- HNO_3 -25 °C and CF- HNO_3 -60 °C samples also showed the same trend, and the higher the processing time, the higher the I_D/I_G ratio was.

3.4 Surface chemistry by XPS

The surface chemical composition of UHMCFs before and after HNO_3 oxidation was investigated by XPS, and Fig. 6 shows high-resolution XPS spectra of untreated and surface oxidized UHMCFs. The characteristic peaks in the XPS spectra of untreated and surface oxidized UHMCFs at 284.6 eV, 532.6 eV and 102.6 eV indicated the C_{1s} peak, O_{1s} peak and Si_{2p} peak, respectively, which proved that surface chemical elements of both untreated and oxidized UHMCFs were mainly composed of carbon, oxygen and silicon.

Changes in the relative contents of chemical elements before and after HNO_3 treatment are shown in Table 3. To identify the obvious changes in surface chemical activity,

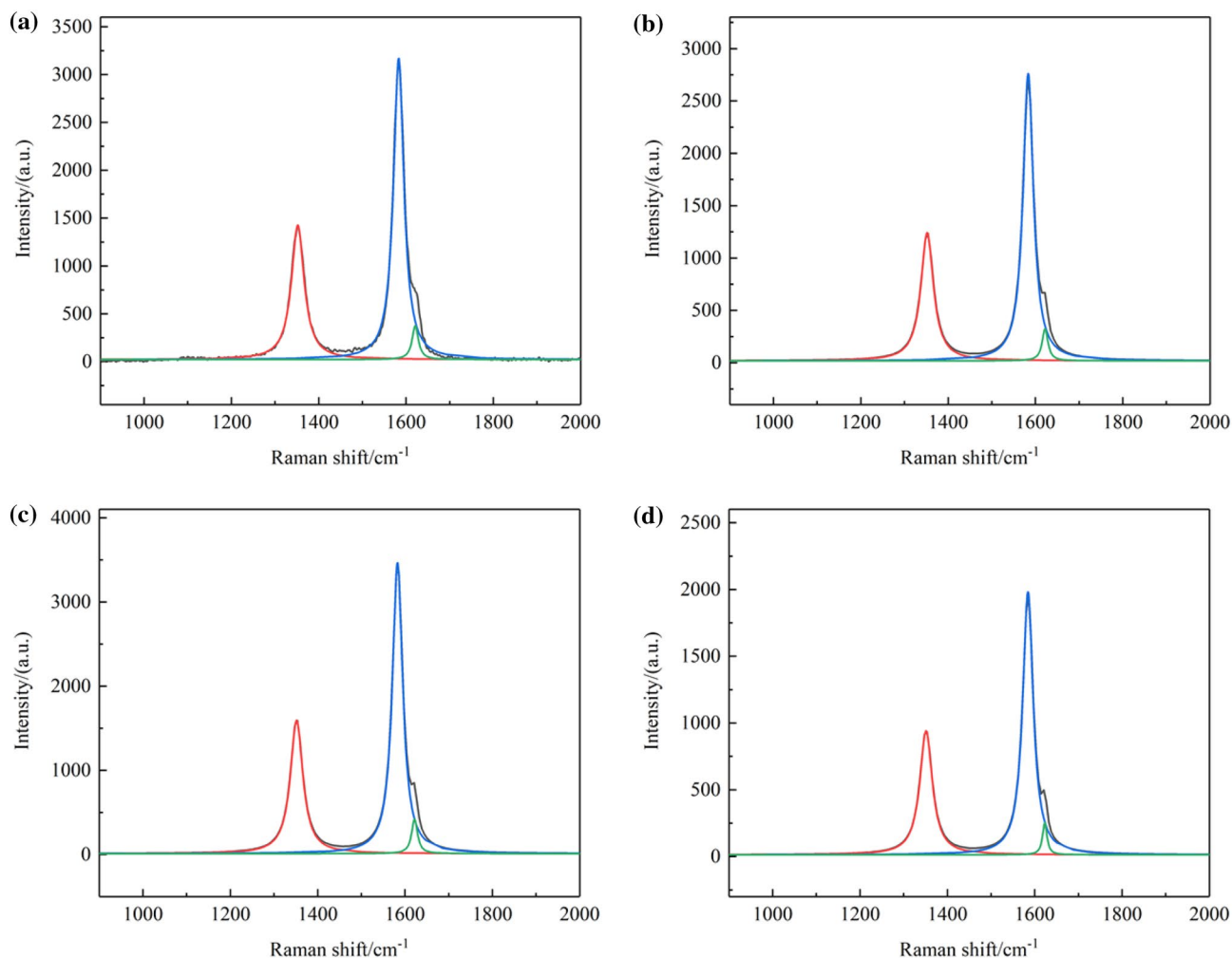


Fig. 4 Raman spectra and their corresponding fitting curves of **a** CF-untreated, **b** CF-HNO₃-25 °C-1 h, **c** CF-HNO₃-60 °C-1 h, **(d)** CF-HNO₃-80 °C-1 h

Table 2 Raman spectrum parameters of UHMCFs with different HNO₃ treatment

Samples	D line		G line		$R (I_D/I_G)$
	Position (cm ⁻¹)	FWHM (cm ⁻¹)	Position (cm ⁻¹)	FWHM (cm ⁻¹)	
CF-untreated	1352.03	35.44	1583.30	28.82	0.528
CF-HNO ₃ -25 °C-0.5 h	1352.04	34.01	1583.31	27.97	0.534
CF-HNO ₃ -60 °C-0.5 h	1351.09	34.54	1583.16	27.50	0.542
CF-HNO ₃ -80 °C-0.5 h	1351.55	34.41	1582.93	28.06	0.550
CF-HNO ₃ -25 °C-1 h	1352.03	34.87	1583.51	28.76	0.549
CF-HNO ₃ -60 °C-1 h	1351.76	34.61	1582.93	28.62	0.555
CF-HNO ₃ -80 °C-1 h	1351.23	34.77	1583.55	29.03	0.565
CF-HNO ₃ -25 °C-2 h	1351.50	35.49	1583.15	28.88	0.567
CF-HNO ₃ -60 °C-2 h	1351.77	34.42	1582.93	28.55	0.575
CF-HNO ₃ -80 °C-2 h	1351.23	34.45	1583.12	28.94	0.585

the O/C ratio on the surface of oxidized UHMCFs are also reviewed in Table 3. The relative contents of C and O elements of untreated UHMCFs were 87.03% and 9.26%,

respectively. The presence of O possibly resulted from absorbed oxygen element in the form CO₂/O₂ after high-temperature treatment.

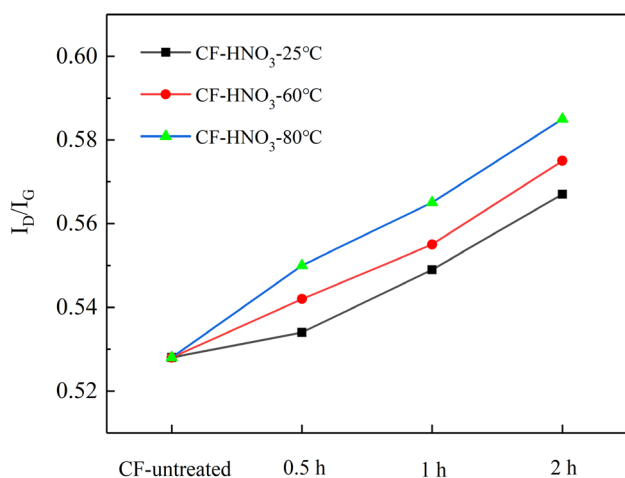


Fig. 5 Relationship between I_D/I_G values, the processing time and the temperature of HNO_3 oxidation

As UHMCFs were oxidized at room temperature, the oxygen percentage of CF-HNO₃-0.5 h sample slightly decreased compared with untreated UHMCFs, which possibly resulted from the elimination of absorbed oxygen element. Obvious increases happened to the oxygen percentages of CF-HNO₃-60 °C-0.5 h and CF-HNO₃-80 °C-0.5 h samples at the expense of carbon elements. Meantime, the O/C ratio of oxidized UHMCFs at 80 °C increased from 0.11 to 0.18, which confirmed that HNO₃ oxidation at higher temperature was much more intense than that at room temperature.

As can be also seen in Table 3, the oxygen percentages of oxidized UHMCFs at 80 °C with the time of 1 h and 2 h decreased compared that of 0.5 h, which indicated that higher level of HNO₃ oxidation with increased treating time could result in decreases in surface chemical functionality. This could be due to the excessive oxidation of the UHMCFs surface. High temperature or processing time resulted in the decomposition of the carbon double bond on the surface of UHMCFs into [H] and CO₂ (as shown in Scheme 1) [47]. As a result, the corresponding O/C ratio decreased.

The chemical composition results showed a certain regularity as the processing time was 0.5 h. Therefore, high-resolution XPS C1s spectra and fitting curves of UHMCFs under HNO₃ treatment with the process time of 0.5 h are shown in Fig. 7. The XPS spectra of the C1s region is deconvoluted into four kinds of carbon-based functional groups: graphite carbon (C–C, 284.6 eV), carbon atoms in hydroxyl group or ether bond (C–OH, 285.5 ± 0.2 eV), carbon atoms in carbonyl group (C=O, 286.6 ± 0.3 eV), and carbon atoms in carboxyl or ester group (–COOH, 289.3 ± 0.2 eV) [48–50].

The calculated percentages of graphitic carbon and oxygen-containing functional groups on the surface of untreated and surface oxidized UHMCFs are listed in Table 4. The calculated percentages of C=O groups was as high as

11.56% on the surface of untreated UHMCFs. According to the results by our previous research, the basic C=O groups couldn't react with the functional groups of epoxy resin and –COOH groups were responsible for the strong reactions between CF surfaces and the epoxy resin in the preparation of CF/epoxy composites [51]. Compared with untreated UHMCFs (CF-0), significant decreases in the relative content of the C=O group showed up on the surfaces of oxidized UHMCFs. The relative content of the –COOH group also increased which was beneficial to the interfacial chemical reaction in the preparation of UHMCF/epoxy resin composites.

3.5 Surface wettability analysis and interfacial shear strength

Figure 8 shows the contact angle and surface energy values of untreated and surface oxidized UHMCFs (processing time 1 h). According to the surface materialization principle, the size of contact angle is closely related to the infiltration of the infiltrating fluid to the fibers [11, 13]. Generally speaking, the smaller the contact angle and the higher the surface energy, the better the wettability of the resin to the fibers [37].

As shown in Fig. 8a, the contact angles between untreated UHMCFs and the water as well as diiodomethane were 72.42° and 49.42°, respectively. The contact angles between oxidized UHMCFs and the water as well as diiodomethane decreased. Especially for the oxidized UHMCFs at 80 °C, the contact angles between the CF-HNO₃-80 °C sample and the diiodomethane decreased from 49.42° to 30.37°, which indicated that HNO₃ surface treatment could improve the surface wettability of UHMCFs.

As for surface energy of UHMCFs before and after HNO₃ oxidation, it can be seen from Fig. 8b that HNO₃ surface treatment even at 25 °C could also improve the surface energy of UHMCFs. The total surface energy of UHMCFs increased from 42.39 mN/m of untreated UHMCFs to 50.02 mN/m of CF-HNO₃ sample. On the other hand, increased treating temperature was beneficial to increases in fiber surface energy. When the UHMCFs oxidized at 80 °C, the total surface energy increased by 27.7% compared with untreated UHMCFs.

3.6 Mechanical properties of UHMCFs and UHMCF/EP composites

Figure 9 reveals the mechanical properties of UHMCFs before and after HNO₃ treatment. Compared with untreated UHMCFs, HNO₃ surface treatment resulted in significant decreases in the tensile modulus (Fig. 9a). Increased processing temperature and time resulted in significant decreases in the modulus, e.g., the tensile modulus of

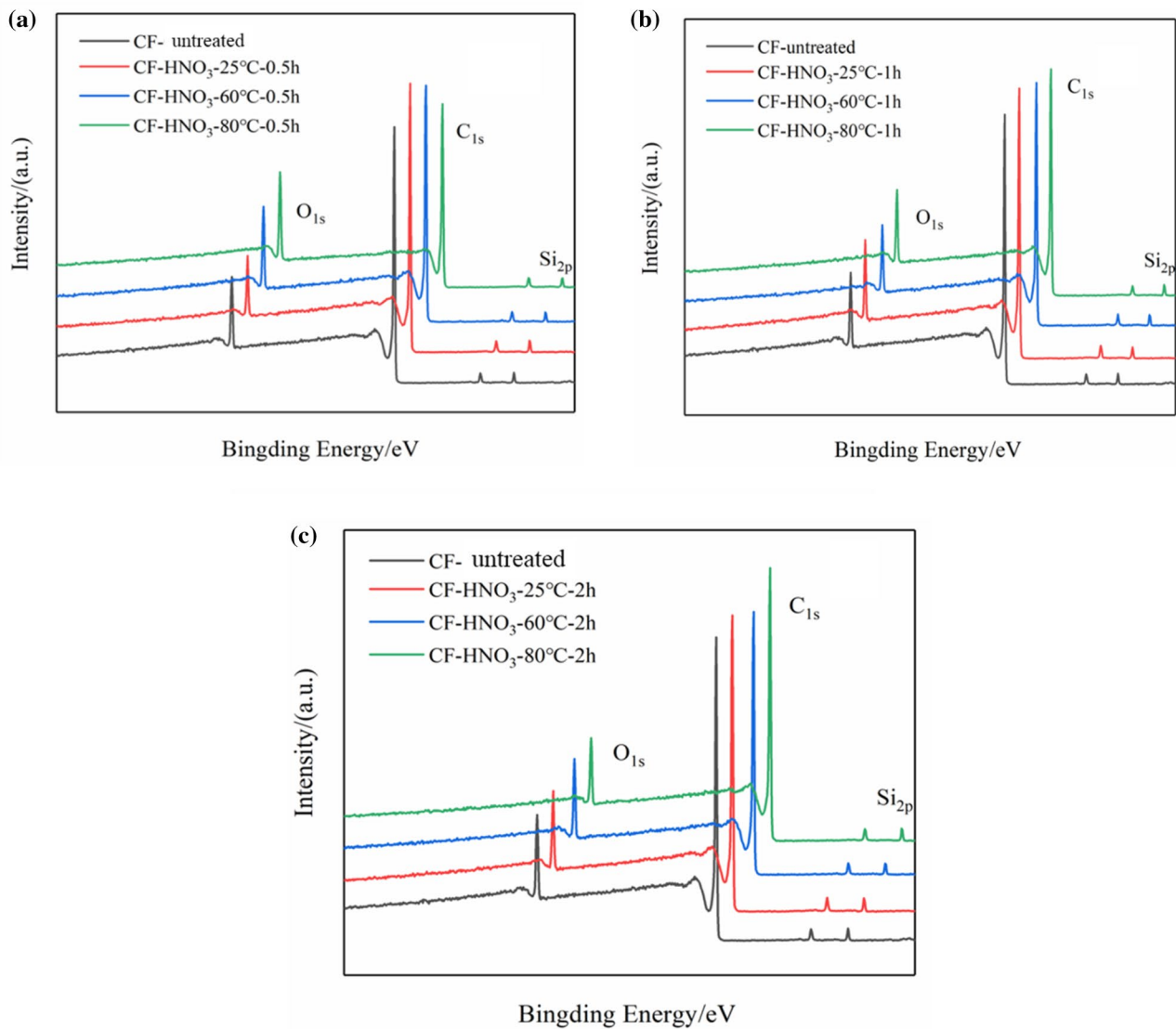


Fig. 6 High-resolution XPS spectra of **a** processing time was 0.5 h, **b** processing time was 1.0 h, **c** processing time was 2.0 h

Table 3 Surface elemental and chemical composition of UHMCFs

Samples	Relative contents of chemical element (%)			Atomic ratio (O/C)
	C _{1s}	O _{1s}	Si _{2p}	
CF-untreated	87.29	9.29	3.42	0.11
CF-HNO ₃ -25 °C-0.5 h	88.05	7.59	4.36	0.09
CF-HNO ₃ -60 °C-0.5 h	85.55	11.13	3.32	0.13
CF-HNO ₃ -80 °C-0.5 h	81.17	14.51	4.32	0.18
CF-HNO ₃ -25 °C-1.0 h	86.14	9.53	4.33	0.11
CF-HNO ₃ -60 °C-1.0 h	87.19	8.86	3.95	0.10
CF-HNO ₃ -80 °C-1 h	86.26	9.88	3.86	0.11
CF-HNO ₃ -25 °C-2 h	87.52	8.28	4.20	0.10
CF-HNO ₃ -60 °C-2 h	86.70	9.48	3.82	0.11
CF-HNO ₃ -80 °C-2 h	87.84	7.97	3.95	0.09

CF-HNO₃-25 °C-2 h (463.34 GPa) decreased by 6.14% compared with untreated UHMCFs (493.65 GPa). A large extent of decline in the fiber modulus showed up as treatment temperature increased to 80 °C and the tensile modulus of CF-HNO₃-80 °C-2 h decreased by about 10.68% compared with untreated UHMCFs. However, the effects of both the processing temperature and time on the tensile strength of oxidized UHMCFs were not obvious (as shown in Fig. 9b).

The IFSS values of UHMCF/epoxy resin composites before and after HNO₃ treatment (processing time 1 h) is shown in Fig. 10. Due to highly inert surface of untreated UHMCFs, the IFSS value of composites reinforced by untreated UHMCFs was only 14.59 MPa. Compared with untreated UHMCFs, the IFSS value of composites reinforced by CF-HNO₃-80 °C increased by 25.7%. Increases

Scheme 1 The oxidative process of HNO_3 oxidation treatment

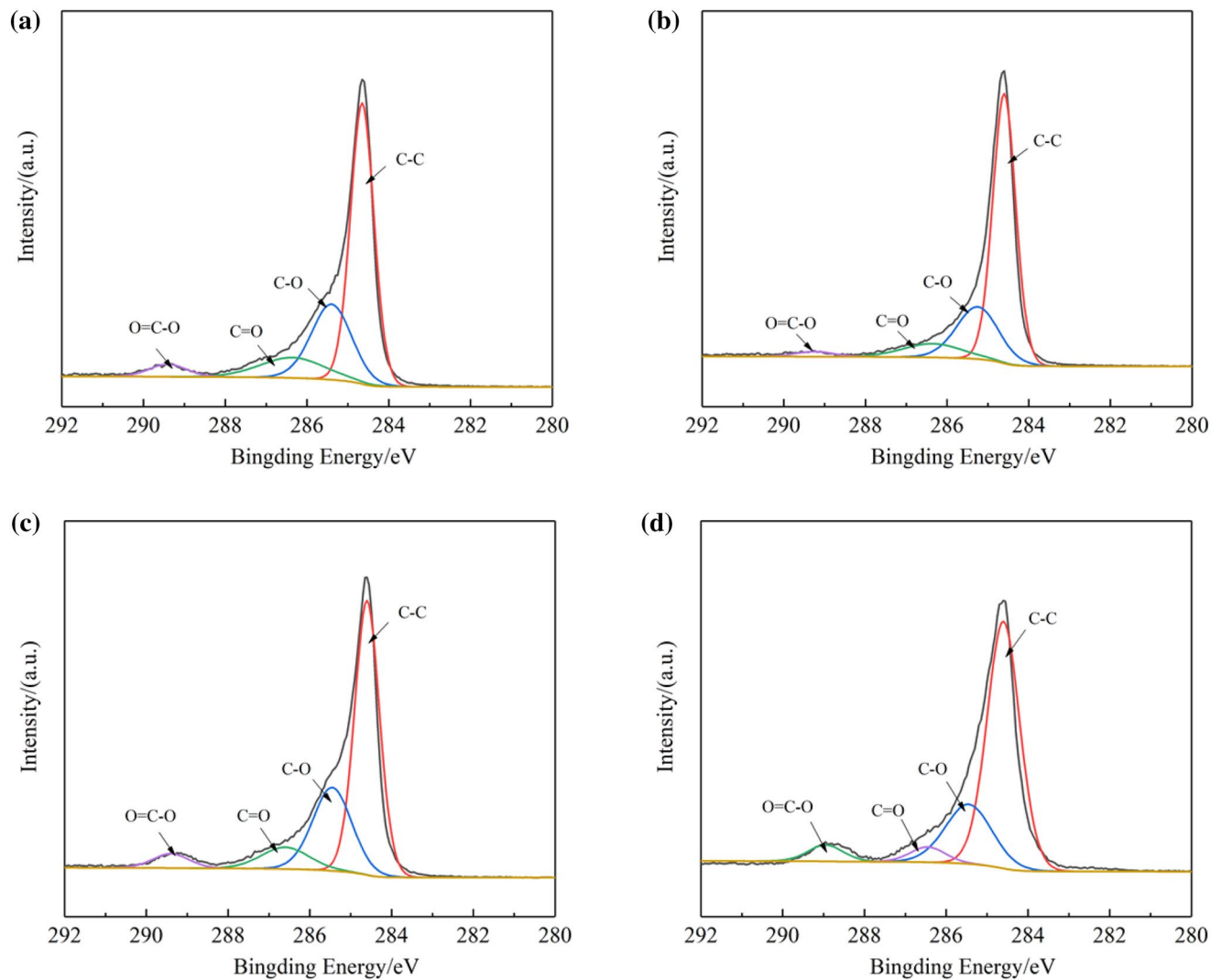
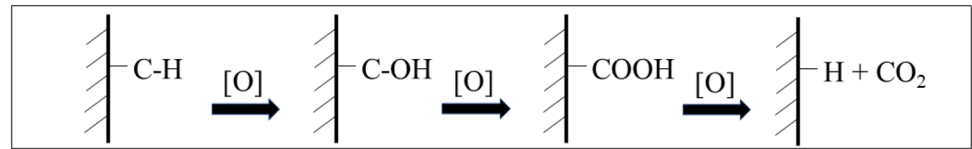


Fig. 7 High-resolution XPS C1s spectra and fitting curves of **a** CF-untreated, **b** CF- HNO_3 -25 °C-0.5 h, **c** CF- HNO_3 -60 °C-0.5 h, **d** CF- HNO_3 -80 °C-0.5 h

in the IFSS values could be due to increased fiber surface activity and functionality [52], and results in the paper also showed that HNO_3 surface treatment of UHMCFs could enhance the interfacial properties of UHMCF/epoxy resin composites.

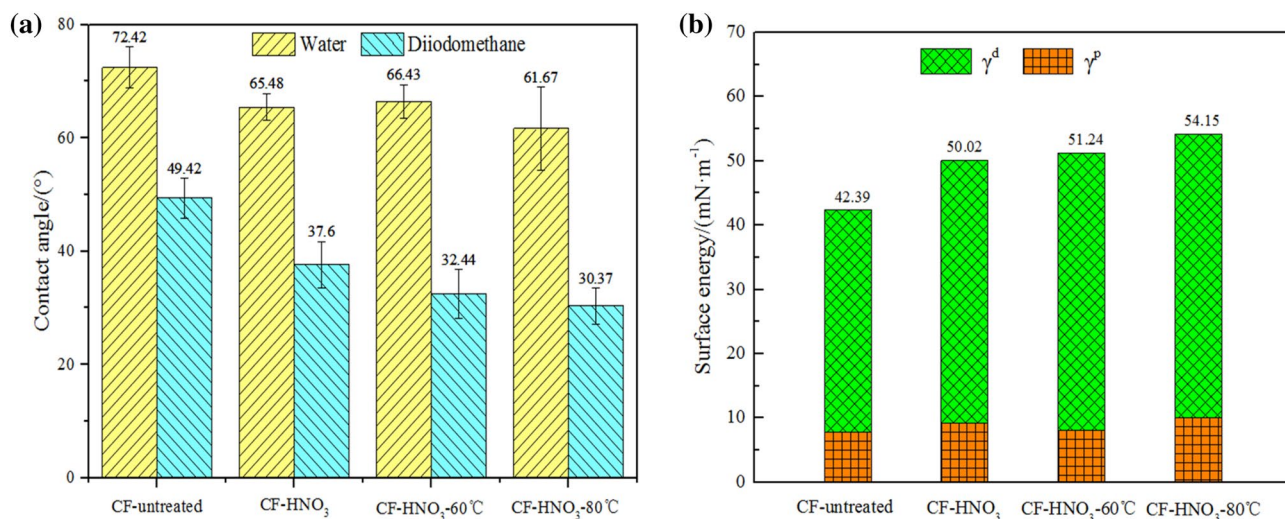
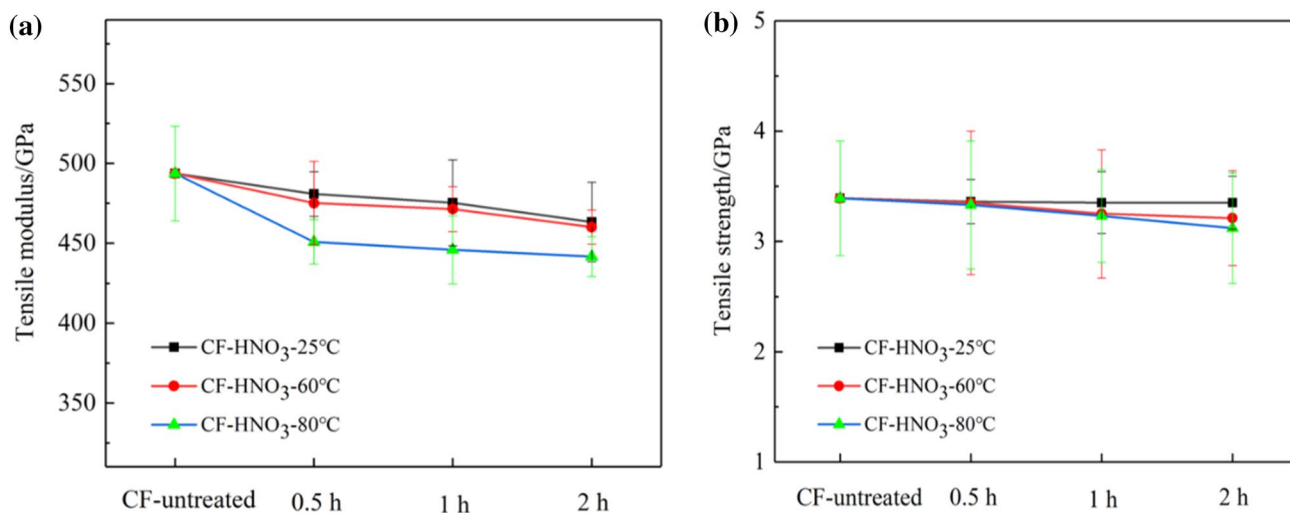
3.7 Effect of HNO_3 oxidation on the mechanical properties of UHMCFs

The typical skin–core structure of high performance CFs has been proved in early published documents [53–55], and

Table 4 Relative contents of graphitic and functional groups on the UHMCf surfaces

Samples	C–C (%)	C–OH (%)	C=O (%)	–COOH (%)
CF-untreated	57.68	26.71	11.56	4.05
CF-HNO ₃ -25 °C-0.5 h	65.80	23.40	8.69	2.11
CF-HNO ₃ -60 °C-0.5 h	58.65	27.89	8.99	4.48
CF-HNO ₃ -80 °C-0.5 h	67.47	23.24	4.81	4.47

it is also well-known that the graphitic structure does exist in CFs, but the bulk of the material is in the turbostratic form [55]. In the preparation of UHMCf, the turbostratic structure of CFs gradually turn to the graphitic structure of UHMCf. However, there still exists turbostratic structure in the UHMCf which was proved by above XRD results. Due to the skin–core structure, the graphitic structure on external surface of UHMCf more easily formed and increased. The micro-structure of UHMCf before and after HNO₃ oxidation is shown in Fig. 11. The tensile modulus of

**Fig. 8** Value of **a** the contact angle, **b** the surface energy of untreated and oxidized UHMCf**Fig. 9** Mechanical properties of UHMCf before and after HNO₃ oxidation

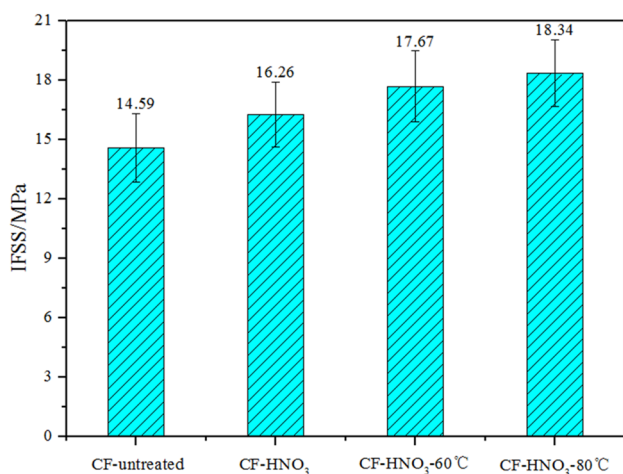


Fig. 10 Interfacial shear strength of UHMCF/epoxy resin composites

UHMCFs is highly dependent on the graphite structure, and the tensile modulus increases significantly with decreases in the d_{002} value and improvements in the Lc value [29]. As shown in Table 1 and Fig. 3, the d_{002} value of oxidized UHMCFs increased and the Lc value of oxidized UHMCFs also decreased due to chemical etching during the HNO₃ oxidation. As a result, significant decreases happened to the tensile modulus of UHMCFs after HNO₃ oxidation (Fig. 9a).

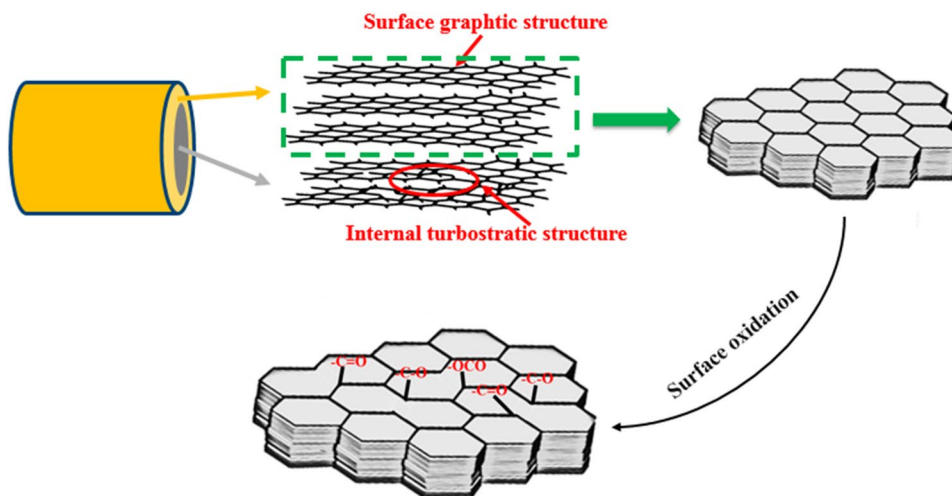
As for the tensile strength of UHMCFs, it is more likely related to the turbostratic structure. A large Lc value could

be accompanied by reduced lateral bonding between the stacks of carbon layers, thereby degrading the strength [29]. In other words, decreased Lc value of oxidized UHMCFs due to HNO₃ oxidation had a positive effect on fiber strength. HNO₃ oxidation could result in a certain degree of decline in the tensile strength of UHMCFs, but it merely affected the external surfaces of UHMCFs (as shown in Fig. 11). As a result, effect of the HNO₃ oxidation on the tensile strength was not obvious (Fig. 9b).

4 Conclusions

The highly inert surfaces of UHMCFs results in poor interfacial properties between UHMCFs and epoxy matrix. In the present article, the HNO₃ oxidation of UHMCFs was conducted to improve UHMCFs surface activity. Compared with the untreated UHMCFs, the HNO₃ oxidation of UHMCFs resulted in decreases in the graphitization degree, and UHMCFs surface became much more activity and functionality after surface oxidation. Significant decreases happened to the tensile modulus of UHMCFs after the HNO₃ oxidation as the treating temperature and the treating time increased. However, HNO₃ oxidation treatment had no significant effect on the tensile strength, After the HNO₃ oxidation treatment, the highest IFSS value of composites reinforced by oxidized UHMCFs increased by 25.7%.

Fig. 11 Micro-structure of UHMCFs before and after HNO₃ oxidation



Acknowledgements The authors would like to acknowledge the financial supports from Equipment Development Fund in The Field of Key Projects (no. 6140922010103), the Strategic Priority Research of Programme of Chinese Academy of Sciences (No. XDA17020405), Natural Science Foundation of Zhejiang Province (no. LY18E080037), and the “Science and Technology Innovation 2025” Major Project of Ningbo of China (no. 2019B10091).

References

- Sharma M, Gao S, Mäder E et al (2014) Carbon fiber surfaces and composite interphases. *Compos Sci Technol* 102:35–50
- Raphael N, Namratha K, Chandrashekar BN et al (2018) Surface modification and grafting of carbon fibers: a route to better interface. *Prog Cryst Growth Charact Mater* 64:75–101
- Kim KW, Jeong JS, An KH et al (2019) A study on the microstructural changes and mechanical behaviors of carbon fibers induced by optimized electrochemical etching. *Compos Part B Eng* 165:764–771
- Werken N, Reese MS, Taha MR et al (2019) Investigating the effects of fiber surface treatment and alignment on mechanical properties of recycled carbon fiber composites. *Compos Part A Appl Sci Manuf* 119:38–47
- Zhang RL, Huang YD, Liu L et al (2011) Effect of the molecular weight of sizing agent on the surface of carbon fibres and interface of its composites. *Appl Surf Sci* 257:1840–1844
- Lissek F, Haeger A, Knoblauch V et al (2018) Acoustic emission for interlaminar toughness testing of CFRP: evaluation of the crack growth due to burst analysis. *Compos Part B Eng* 136:55–62
- Liu L, Jia C, He J et al (2015) Interfacial characterization, control and modification of carbon fiber reinforced polymer composites. *Compos Sci Technol* 121:56–72
- Newcomb BA (2016) Processing, structure, and properties of carbon fibers. *Compos Part A Appl Sci Manuf* 91:262–282
- Yue Z, Vakili A, Duran MP (2017) Surface treatments of solvated mesophase pitch-based carbon fibers. *J Mater Sci* 52:10250–10260
- Wen Z, Xu C, Qian X et al (2019) A two-step carbon fiber surface treatment and its effect on the interfacial properties of CF/EP composites: the electrochemical oxidation followed by grafting of silane coupling agent. *Appl Surf Sci* 486:546–554
- Zhang Y, Choi JR, Park SJ (2018) Enhancing the heat and load transfer efficiency by optimizing the interface of hexagonal boron nitride/elastomer nanocomposites for thermal management applications. *Polymer* 143:1–9
- Sun T, Li M, Zhou S et al (2020) Multi-scale structure construction of carbon fiber surface by electrophoretic deposition and electropolymerization to enhance the interfacial strength of epoxy resin composites. *Appl Surf Sci* 499:143929
- Wen Z, Qian X, Zhang Y et al (2019) Electrochemical polymerization of carbon fibers and its effect on the interfacial properties of carbon reinforced epoxy resin composites. *Compos Part A Appl Sci Manuf* 119:21–29
- Du X, Xu F, Liu HY et al (2016) Improving the electrical conductivity and interface properties of carbon fiber/epoxy composites by low temperature flame growth of carbon nanotubes. *RSC Adv* 6:48896–48904
- Lutz V, Duchet-Rumeau J, Godin N et al (2018) Ex-PAN carbon fibers vs carbon nanotubes fibers: from conventional epoxy based composites to multiscale composites. *Eur Polym J* 106:9–18
- Barzoki PK, Rezadoust AM, Latifi M et al (2018) The experimental and numerical study on the effect of PVB nanofiber mat thickness on interlaminar fracture toughness of glass/phenolic composites. *Eng Fract Mech* 194:145–153
- Xiao C, Tan Y, Wang X et al (2018) Study on interfacial and mechanical improvement of carbon fiber/epoxy composites by depositing multi-walled carbon nanotubes on fibers. *Chem Phys Lett* 703:8–16
- Chang H, Luo J, Liu HC et al (2019) Carbon fibers from polyacrylonitrile/cellulose nanocrystal nanocomposite fibers. *Carbon* 145:764–771
- Rostamiyan Y, Youseftabar H, Azadi R (2018) Experimental study on the effect of nano zirconia on mechanical strength and microstructure of damaged epoxy-nanocomposites. *Mater Res Express* 6:025046
- Qian X, Wang X, OuYang Q et al (2012) Surface structural evolution in electrochemical oxidation and sizing and its effect on carbon fiber/epoxy composites properties. *J Reinf Plast Compos* 31:999–1008
- Qian X, Zhi J, Chen L et al (2013) Effect of low current density electrochemical oxidation on the properties of carbon fiber-reinforced epoxy resin composites. *Surf Interface Anal* 45:937–942
- Zhang G, Sun S, Yang D et al (2008) The surface analytical characterization of carbon fibers functionalized by H₂SO₄/HNO₃ treatment. *Carbon* 46:196–205
- Paredes JI, Martinez-Alonso A, Tascon JMD (2003) Atomic-scale scanning tunneling microscopy study of plasma-oxidized ultrahigh-modulus carbon fiber surfaces. *J Colloid Interface Sci* 258:276–282
- Lee ES, Lee CH, Chun YS et al (2017) Effect of hydrogen plasma-mediated surface modification of carbon fibers on the mechanical properties of carbon-fiber-reinforced polyetherimide composites. *Compos Part B Eng* 116:451–458
- Moosburger-Will J, Lachner E, Löffler M et al (2018) Adhesion of carbon fibers to amine hardened epoxy resin: influence of ammonia plasma functionalization of carbon fibers. *Appl Surf Sci* 453:141–152
- Yuan JM, Fan ZF, Yang QC et al (2018) Surface modification of carbon fibers by microwave etching for epoxy resin composite. *Compos Sci Technol* 164:222–228
- Woodhead AL, Souza ML, Church JS (2017) An investigation into the surface heterogeneity of nitric acid oxidized carbon fiber. *Appl Surf Sci* 401:79–88
- Chae HG, Newcomb B, Gulgunje PV et al (2015) High strength and high modulus carbon fibers. *Carbon* 93:81–87
- Qian X, Zhi J, Chen L et al (2018) Evolution of microstructure and electrical property in the conversion of high strength carbon fiber to high modulus and ultrahigh modulus carbon fiber. *Compos Part A Appl S* 112:111–118
- Qian X, Zhong J, Zhi J et al (2019) Electrochemical surface modification of polyacrylonitrile-based ultrahigh modulus carbon fibers and its effect on the interfacial properties of UHMCF/EP composites. *Compos Part B Eng* 164:476–484
- Kiuchi N, Sohda Y, Arai Y et al (2000) Unique low modulus carbon fibers for hybrid materials with excellent impact resistance. In: *SAMPE 2000: 45 th International SAMPE Symposium and Exhibition* 330–341
- Anikin VA, Andrianova NN, Borisov AM et al (2017) Physical and mechanical properties of high-modulus carbon fiber crimped by ion irradiation. *J Phys Conf Ser* 941:102029
- Xu P, Yu Y, Liu D et al (2018) Enhanced interfacial and mechanical properties of high-modulus carbon fiber composites: establishing modulus intermediate layer between fiber and matrix based on tailored-modulus epoxy. *Compos Sci Technol* 163:26–33
- Makeev A, Ghaffari S, Seon G (2019) Improving compressive strength of high modulus carbon-fiber reinforced polymeric composites through fiber hybridization. *Int J Eng Sci* 142:145–157

35. Zhao XJ, Qin W, Wang BL (2007) Effect of ozone treatment on the interfacial properties of high modulus carbon fiber/epoxy composites. *Mater Sci Forum* 546–549:1547–1550
36. Zhang T, Qi L, Li S et al (2019) Evaluation of the effect of PyC coating thickness on the mechanical properties of T700 carbon fiber tows. *Appl Surf Sci* 463:310–321
37. Ma L, Li N, Wu G et al (2018) Interfacial enhancement of carbon fiber composites by growing TiO₂ nanowires onto amine-based functionalized carbon fiber surface in supercritical water. *Appl Surf Sci* 433:560–567
38. Jiang D, Xing L, Liu L et al (2015) Enhanced mechanical properties and anti-hydrothermal ageing behaviors of unsaturated polyester composites by carbon fibers interfaced with POSS. *Compos Sci Technol* 117:168–175
39. Li WW, Kang HL, Xu J et al (2018) Microstructures of high-strength high-modulus carbon fibers and high-modulus carbon fibers. *Acta Polym Sin* 49:380–388
40. Chen X, Zha L, Zhu Y (2010) Microstructure of high tensile strength and high tensile modulus PAN-based carbon fibers determined by X-ray diffraction. *New Chem Mater* 38:85–88
41. Hao W, Wang Z, Zhang X et al (2018) Transforming of high-strength-medium-modulus into high-modulus carbon fiber. *New Chem Mater* 46:70
42. Qian X, Wang X, Zheng K et al (2019) Relationship between micro-structure and macro-properties during the formation of PAN-based high modulus carbon fibers. *Chem Ind Eng Prog* 38:2276–2283
43. Melanitis N, Tetlow PL, Galiotis C (1996) Characterization of PAN-based carbon fibres with laser Raman spectroscopy. 1. Effect of processing variables on Raman band profiles. *J Mater Sci* 31:851–860
44. Moosburger-Will J, Jan J, Strauch J et al (2016) Interphase formation and fiber matrix adhesion in carbon fiber reinforced epoxy resin: influence of carbon fiber surface chemistry. *Compos Interfaces* 24:1–20
45. Ren GZ, Chen CJ, Deng LH et al (2015) Microstructural heterogeneity on the cylindrical surface of carbon fibers analyzed by Raman spectroscopy. *New Carbon Mater* 30:476–480
46. Qian X, Wang X, Zhong J et al (2019) Effect of fiber microstructure studied by Raman spectroscopy upon the mechanical properties of carbon fibers. *J Raman Spectrosc* 50:665–673
47. Fu Y, Lu Y, You T et al (2019) Study on multistage anodization for high-modulus carbon fiber. *Surf Interface Anal* 51:798–808
48. Paiva MC, Bernardo CA, Nardin M (2000) Mechanical, surface and interfacial characterisation of pitch and PAN-based carbon fibres. *Carbon* 38:1323–1337
49. Liu X, Yang C, Lu Y (2012) Contrastive study of anodic oxidation on carbon fibers and graphite fibers. *Appl Surf Sci* 258:4268–4275
50. Wang B, Duan Y, Zhang J et al (2016) Microwave radiation effects on carbon fibres interfacial performance. *Compos Part B Eng* 99:398–406
51. Qian X, Chen L, Huang J et al (2013) Effect of carbon fiber surface chemistry on the interfacial properties of carbon fibers/epoxy resin composites. *J Reinf Plast Compos* 32:393–401
52. Guigon M, Oberlin A, Desarmot G (1984) Microtexture and structure of some high-modulus, PAN-base carbon fibres. *Fibre Sci Technol* 20:177–198
53. Guigon M, Oberlin A, Desarmot G (1984) Microtexture and structure of some high tensile strength, PAN-base carbon fibres. *Fibre Sci Technol* 20:55–72
54. Peebles LH (1994) Carbon fibres: structure and mechanical properties. *Int Mater Rev* 39:75–92
55. Zhang T, Cheng Q, Xu Z et al (2019) Improved interfacial property of carbon fiber composites with carbon nanotube and graphene oxide as multi-scale synergetic reinforcements. *Compos Part A Appl Sci Manuf* 125:105573

Publisher's Note Springer Nature remains neutral with regard to jurisdictional claims in published maps and institutional affiliations.